Min Zhang and Qiangchun Liu*

Solvothermal Synthesis and Magnetic Properties of Monodisperse $Ni_{0.5}Zn_{0.5}Fe_2O_4$ Hollow Nanospheres

https://doi.org/10.1515/htmp-2017-0101
Received July 15, 2017; accepted June 04, 2018

Abstract: The monodisperse $Ni_{0.5}Zn_{0.5}Fe_2O_4$ nanospheres have been synthesized via a simple solvothermal method. The effects of reactant concentration on structural and magnetic properties have been studied. X-ray diffraction analysis results indicate that the lattice constant and crystallite size can be tuned by controlling reactant concentration. The nanosphere size monotonically decreases from 238 to 35 nm with increasing reactant concentration. The magnetic studies show that blocking temperature is enhanced, and these single-domain particles are superparamagnetism at room temperature. The hollow nanospheres exhibit a high saturation magnetization value of 52.6 emu/g. The nanospheres with various diameters exhibit different magnetic saturation values which may be caused by the domain structure, surface effects and the distribution of metal ions on A and B sites. These superparamagnetic $Ni_{0.5}Zn_{0.5}Fe_2O_4$ nanospheres are expected to have potential application in biomedicine and magnetic fluid technology.

Keywords: Ni–Zn ferrite, solvothermal method, blocking temperature, superparamagnetic behavior

Introduction

Nickel–zinc ferrite (Ni–Zn ferrite) is one of the most versatile magnetic materials due to the high saturation magnetization, high Curie temperature, excellent chemical stability, low coercivity and biodegradability [1]. It is a mixed spinel structure based on a face-centered cubic lattice of oxygen ions, with functional units of $(Zn_xFe_{1-x})[Ni_{1-x}Fe_{1+x}]O_4$. Zn^{2+} and Ni^{2+} ions are known to have very strong preferences for the tetrahedral A and octahedral B sites as depicted by curled and square brackets [2], respectively, while Fe^{3+} ions partially occupy the A and B sites. In the case of $Ni_xZn_{1-x}Fe_2O_4$ system, it was found that for x greater than 0.5, Fe^{3+} moments in A and B sites have collinear arrangement, whereas for x less than 0.5, Fe^{3+} moments in the B site have noncollinear arrangement [3]. In our previous studies [4], it is found that $Ni_{0.5}Zn_{0.5}Fe_2O_4$ presents the best magnetic properties and microwave absorption ability in the $Ni_{1-x}Zn_xFe_2O_4$ system. Thus, it is necessary to further study the microstructure and magnetic properties of $Ni_{0.5}Zn_{0.5}Fe_2O_4$ nanoparticles.

Various wet chemical synthesis have been used to prepare nanosized Ni–Zn ferrite powders such as the co-precipitation method [5, 6], hydrothermal route [7], reverse micelle process [8] and sol–gel method [9]. Among these methods, the hydrothermal/solvothermal method requires neither expensive starting materials and environment unfriendly solvent nor extremely high temperature and pressure. Hence, the hydrothermal/solvothermal method is usually used to synthesize Ni–Zn ferrites.

Some groups [7, 10] have synthesized the $Ni_{0.5}Zn_{0.5}Fe_2O_4$ sample by hydrothermal method and investigated different morphology and magnetic properties of the spinel ferrite samples by controlling the process parameters such as solution pH value, reaction temperature and durable time. However, few groups have investigated the morphology and magnetic properties by adjusting the reactant concentration. Some templates, such as silica [11] and carbon [12], have been widely investigated to prepare hollow spheres. However, the synthetic process usually suffers from high cost or complicated operation. Gu et al. [12] have reported the synthesis of $CoFe_2O_4$ hollow spheres obtained from hydrothermal treatment of the mixed solution of glucose. It was found that the variation of metal concentration showed little influence on the size of hollow spheres. Recently, considerable attention has been focused on hollow nanostructure without any templates. Jiang et al. [13] have fabricated hollow spheres of $ZnFe_2O_4$ without the assistance of a template by solvothermal method. $ZnFe_2O_4$ exhibited ferromagnetic properties with high

***Corresponding author: Qiangchun Liu,** School of Physics and Electronics Information, Huaibei Normal University, Huaibei 235000, People's Republic of China, E-mail: qchliu@chnu.edu.cn
Min Zhang, School of Physics and Electronics Information, Huaibei Normal University, Huaibei 235000, People's Republic of China

saturation magnetization (M_s) of 83.4 emu/g. The relatively high M_s was induced by the superexchange effect which existed in the site of Zn–O–Fe.

Here, to the best of our knowledge, our group has synthesized monodisperse $Ni_{0.5}Zn_{0.5}Fe_2O_4$ hollow nanospheres without adding any surfactants or templates by controlling the reactant concentration in nonaqueous hydrothermal method. It is the first time to systematically demonstrate the effect of nanosphere size of $Ni_{0.5}Zn_{0.5}Fe_2O_4$ ferrites on the magnetic behaviors. The possible formation mechanism is discussed in detail.

Experimental

The monodisperse $Ni_{0.5}Zn_{0.5}Fe_2O_4$ (NZFO) nanospheres have been prepared using the solvothermal method, reported elsewhere [14]. For simplicity, the NZFO powders obtained under the same reaction conditions of temperature and reaction time, but with different concentrations, are named as NZFO-*A*, where *A* represents the mole number of the as-prepared NZFO powders. For example, NZFO-200 indicates that 0.002 mol NZFO powders were prepared at 180 °C with 24 h.

X-ray diffraction (XRD) patterns of the as-prepared products were recorded on a Philips X'pert PRO x-ray diffractometer with Cu K_α radiation. Field emission scanning electron microscopy (FESEM, FEI Sirion 200) and transmission electron microscopy (TEM, JEM-2010) were used to show the surface morphology and particle size distribution. The magnetic properties of the NZFO ferrite powders were measured by using a superconducting quantum interference device magnetometer measurement system (SQUID, MPMS-5T). The zero-field cooling (ZFC) and field cooling (FC) magnetization curves were performed in the temperature range between 5 and 350 K under an applied magnetic field of 100 Oe.

Results and Discussion

Structure and Morphology

Figure 1 shows the room-temperature XRD patterns and Rietveld analysis results for NZFO ferrite at different reactant concentrations. The parameters R_p (profile fitting *R* value), R_{wp} (weighted profile *R* value) and χ^2 (goodness-of-fit quality factor) obtained after refinement are presented in Figure 1. For an excellent fit, the value of χ^2 should be nearly one. As shown in Figure 1, the value of χ^2 is less than or equal to two. Hence, the good fitting parameters indicate that the studied samples are of better quality and refinements of samples are effective. All reflection peaks have a good agreement with the standard JCPDS card of Ni-Zn ferrite (card no. 08-0234), and no other phase is detectable. The lattice constant *a* is obtained by Rietveld method, as listed Table 1. It is observed that the *a* value obviously increases with the

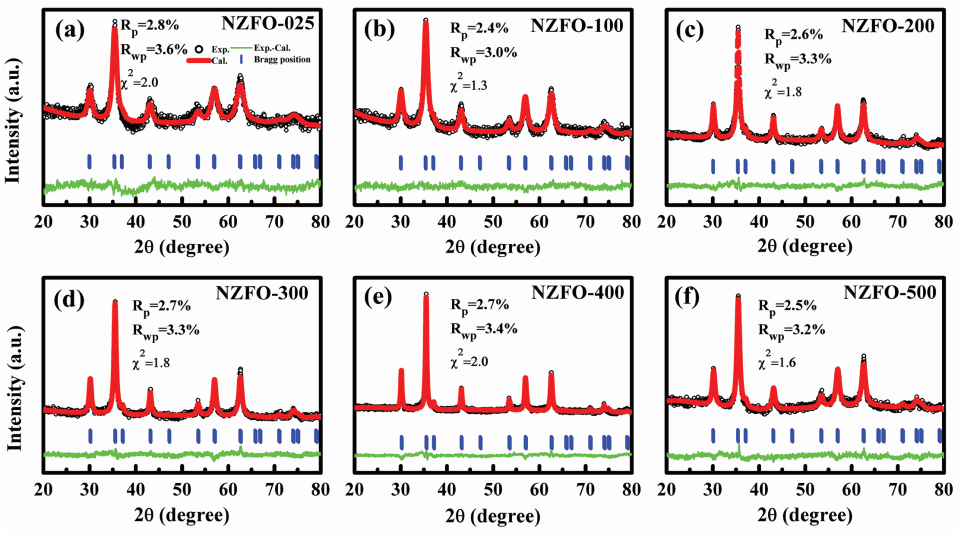

Figure 1: Refined room-temperature XRD patterns of $Ni_{0.5}Zn_{0.5}Fe_2O_4$ with different reactant concentrations. The black circle, red, blue and green lines signals represent the experimental pattern (Exp.), calculated pattern (Cal.), Bragg position and the difference plot (Exp.- Cal.), respectively.

Table 1: Lattice constant a (Å), crystalline size D (nm), nanosphere size (nm), saturation magnetization M_s (emu/g), coercivity H_c (Oe) and blocking temperature (T_B) of the $Ni_{0.5}Zn_{0.5}Fe_2O_4$ samples as a function of the reactant concentration.

Reactant concentration (10^{-3} mol)	Lattice constant (Å)	Crystallite size (nm)	Nanosphere size (nm)	M_s (emu/g) 300 K	H_c (Oe) 300 K	T_B (K)
0.25	8.3683	15	238	...	...	91
1.00	8.3777	17	236	44.5	8.8	134
2.00	8.3796	21	145	46.2	5.1	165
3.00	8.3811	22	125	52.6	2.7	236
4.00	8.3865	31	62	49.0	8.4	> 350
5.00	8.3858	18	35	51.7	10.1	217

increase in reactant concentration, indicating lattice expansion. According to the references [6, 15], we suppose that the variation of lattice constant can be attributed to the cation redistribution between A and B sites. The Zn^{2+}, Ni^{2+} and Fe^{3+} cations simultaneously occupy the A and B sites of the spinel structure. For increasing the reactant concentration, the cation redistribution on A and B sites can increase the ionic radii of A and B sites, resulting in the increase of lattice constant. As shown in Figure 1, the corresponding diffraction peaks become narrower and sharper with increasing concentration of as-prepared NZFO except NZFO-500 sample, which indicates the growth in crystallite and much better crystallinity.

The crystallite size for all NZFO nanoparticles is calculated from intensity (311) peak by the Debye–Scherrer equation:

$$D = \frac{0.9\lambda}{\beta \cos\theta} \quad (1)$$

where D is the crystallite size, λ is the wavelength of Cu K_α ($\lambda = 1.540598$ Å), θ is the angle of Bragg diffraction and β is the full width at half maxima broadening. The values of crystallite size are listed in Table 1, and the variation tendency as a function of reactant concentration is shown in Figure 2. It is observed that crystallite size increases from 15 to 31 nm with increasing concentration, and then decreases to 18 nm as the reactant concentration increases further. The variation of crystallite size as a function of reactant concentration can be attributed to the nucleation and growth of crystals [16]. Once the crystal nuclei are formed, they form a crystal–liquid interface to grow up, namely atoms and ions of component crystals according to the arrangement form of the crystal structure to pile up crystals. The suitable reactant concentration increases the solubility of the crystalline substance and

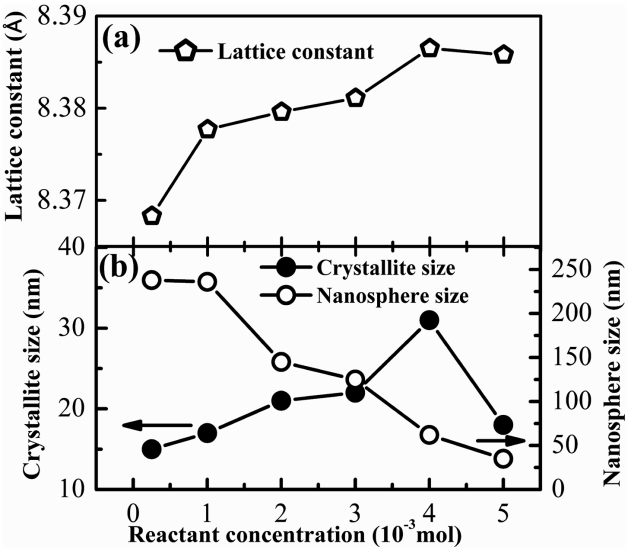

Figure 2: The variations of (a) lattice constant, (b) crystallite size and nanosphere size with the reactant concentration for NZFO samples.

improves the crystal growth rate. So higher reactant concentration accelerates the growth of the crystal. But the excessive reactant concentration can increase the viscosity of the solution and then affect the solute convection, which will inhibit crystal growth. In addition, the decrease in crystallite size could also be related to the higher nucleation rate at higher reactant concentration, causing the consumption of the whole amount of reactants in the solution and stopping the growth of the crystals [17]. As a result, the reactant concentration reaches a critical value of 4 mmol, and then the crystallite size begins to decrease. Thus, the reactant concentration plays an important role in determining the crystallite size.

The microstructure of the NZFO ferrite samples is analyzed by SEM. The surface morphology and the

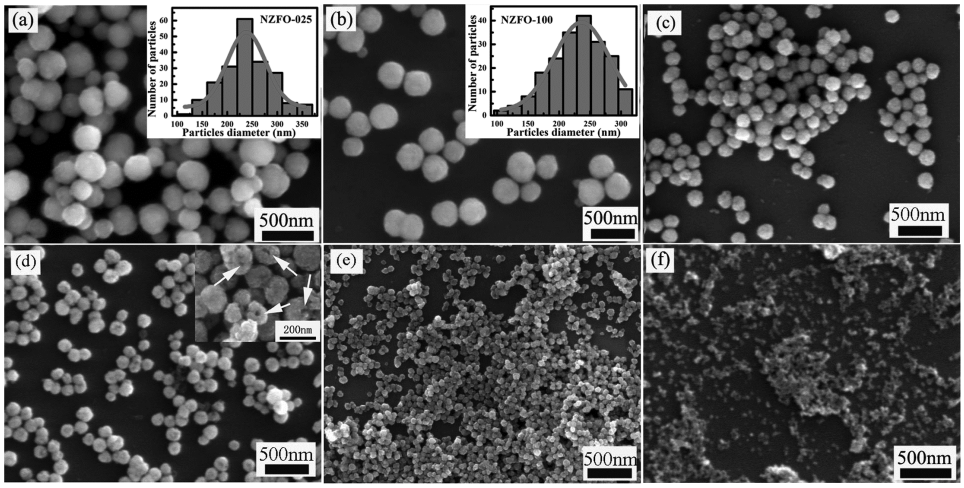

Figure 3: SEM images of NZFO ferrite under different reactant concentrations, the inset is the corresponding particle size distribution graph. (a) NZFO-025, (b) NZFO-100, (c) NZFO-200, (d) NZFO-300, (e) NZFO-400 and (f) NZFO-500.

corresponding nanosphere size distribution graphs of NZFO with different reactant concentrations are shown in Figure 3. The spherical shape can be observed clearly in all samples. It can be clearly seen that the magnetic nanoparticles are agglomerated, but nanospheres consisting of nanoparticles are well monodisperse. The size distribution of the nanospheres was estimated by taking the average of 200 nanospheres and fitting the resultant histogram by a Gaussian function (solid line), as shown in the insets of Figure 3, indicating the size distribution is narrow. The corresponding values of nanosphere size are listed in Table 1. The center of the size distribution curves is shifted from 238 to 35 nm as the concentration increases, as shown in Figure 2, showing the significant influence of the reactant concentration on the nanosphere size. This phenomenon can be explained as the classical theories of crystal heterogeneous nucleation [13]. As indicated by the arrows in the inset of Figure 3 (d), there exist open pores and some broken spheres, indicating the presence of hollow spheres in the NZFO-300 sample. The formation of the hollow NZFO nanospheres can be explained by the Ostwald ripening process [18].

Figure 4 shows the representative TEM images of the NZFO-100 and NZFO-300 samples. Uniform and monodispersed nanospheres are observed. From Figure 4(b), the apparent contrast between the dark edge and the pale center confirms that the NZFO-300 nanospheres have a hollow interior, with the average outer diameter of 135 nm and the wall thickness of 45 nm. The inset of Figure 4(b) reveals clearly that the spherical shell are packed with numerous NZFO nanoparticles, and the average particle diameter is about 20 nm, which verifies the calculating results from XRD data. The insets of Figures 4(a)and 4(b) show the selected area electron diffraction (SAED) pattern. The SAED pattern shows diffuse rings that can be indexed to NZFO [(220), (311), (400), (422), (511), and (440)] plane reflections. High-resolution TEM (HRTEM) analysis is employed to determine the crystal facets and orientation. As shown in Figure 4(c), the lattice fringe spacing of $d = 0.25$ nm agrees well with the (311) lattice plane of cubic NZFO. From Figure 4(d), the results from energy-dispersive x-ray analysis (EDX) spectra show that the as-prepared hollow nanospheres contain Ni, Zn, Fe and O, and no contamination element is detected.

Magnetic Properties

The temperature ($5\,K < T < 350\,K$) dependence of magnetization curves in an external field of 100 Oe recorded in ZFC and FC modes are clearly shown in Figure 5. At first, when the sample is cooled to 5 K without any external magnetic field, the total magnetization of particles will be zero because of randomly oriented magnetic moment. Then, an external magnetic field of 100 Oe is applied, which favors the moment of individual particle to reorient along the applied field at low temperature. With an increase in the temperature, more and more nanoparticles follow the direction of the applied magnetic field and reach the maximum at the blocking temperature (T_B). The ZFC magnetization curves appear maximum at the blocking temperature T_B at which the relaxation time equals the time scale of the magnetization measurements.

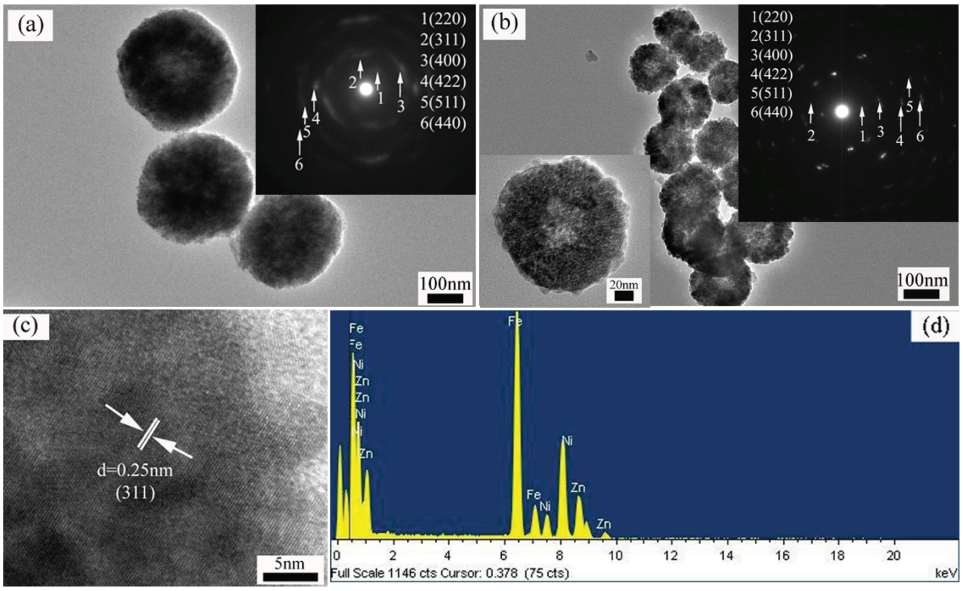

Figure 4: (a) TEM images of the NZFO-100 sample and (b) the NZFO-300 sample. The insets are the corresponding SAED pattern and magnified image; (c) high magnification TEM image of NZFO-300 sample; (d) EDX spectrum of the NZFO-100 sample.

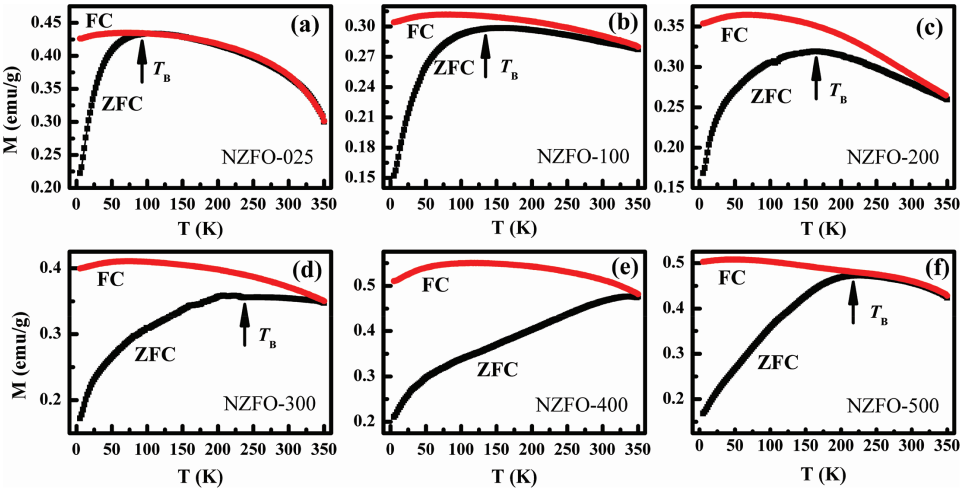

Figure 5: Temperature dependence of magnetization for field cooled (FC) and zero-field cooled (ZFC) NZFO nanoparticles under an applied field of 100 Oe.

Based on the above analysis, the reactant concentration is critical to the particle size. The T_B values of NZFO-025, NZFO-100, NZFO-200, NZFO-300 and NZFO-500 are 91 K, 134 K, 165 K, 236 K and 217 K, respectively, as listed in Table 1, indicating that the different particle sizes are characterized by different average energy barriers. Note that the T_B value of the NZFO-400 sample is higher than 350 K. The value of T_B initially increases with an increase in the reactant concentration, and then decreases as the reactant concentration increases further.

In addition, in the spherical particle model, the critical size from single domain to multidomain can be calculated with the following formula [19]

$$D_m = 9\sigma_w / 2\pi M_s^2 \quad (2)$$

where $\sigma_w = (2k_B T_C |K_1|/a)^{1/2}$ is the domain wall energy, k_B is Boltzmann constant, T_c is Curie temperature, K_1 is the magnetocrystalline anisotropy constant, a is the lattice constant and M_s is the saturation magnetization. The

nanoparticles are considered to be single domain below D_m, while the nanoparticles are multidomain above D_m. For NZFO, $T_c = 538$ K, $a = 8.39 \times 10^{-8}$ cm, $K_1 = 1.7 \times 10^4$ erg/cm^3 and $M_s = 310$ Gs. From eq. (2), the calculation value of D_m is about 26 nm, which is a little less than the one (40 nm) reported by Albuquerque et al. [20]. According to the above analysis, NZFO-400 sample may be multidomain and appear domain wall, but prepared other samples can be considered to be single domain.

According to the Stoner–Wohlfarth theory, the magnetocrystalline anisotropy E_A of a single-domain particle can be expressed as [21]

$$E_A = KV\sin^2\theta \tag{3}$$

where K is the magnetocrystalline anisotropy constant, V is the volume of the nanoparticle and θ is the angle between the magnetic direction and the easy axis of the nanoparticles. The anisotropy acts as the energy barrier to prevent the change of the magnetization direction. When the size of the magnetic nanoparticle is reduced to a threshold value, E_A is comparable with thermal activation energy, k_BT, with k_B as the Boltzmann constant, and the magnetization direction of the nanoparticle can be easily moved away from the easy axis by thermal activation. Above T_B, thermal activation can overcome the anisotropy energy barrier and the nanoparticles become superparamagnetic with the magnetization direction randomly flipping. Below T_B, thermal activation is no longer able to overcome the magnetocrystalline anisotropy of the nanoparticles. According to the above analysis, larger nanoparticles possess a higher E_A, and require a higher k_BT to become superparamagnetic. Therefore, the value of T_B increases with an increase in crystalline size.

The room-temperature magnetic hysteresis loops (*M-H*) of the NZFO nanoparticles prepared with different reactant concentrations are shown Figure 6. The samples exhibit nonsaturated magnetization even at the maximum applied field of 2 T, which indicates the superparamagnetic nature. Above the blocking temperature, the thermal activation can overcome the magnetocrystalline anisotropy, and the magnetocrystalline anisotropy constant may be seen as zero. Consequently, the negligible hysteresis of the nanoparticles is observed, as shown in the inset of Figure 6.

The magnetic moment is obtained using nonlinear curve fit of Langevin function, which is described as the following equations [22]:

$$M = M_s\left(\coth\left(\frac{\mu H}{k_BT}\right) - \frac{k_BT}{\mu H}\right) \tag{4}$$

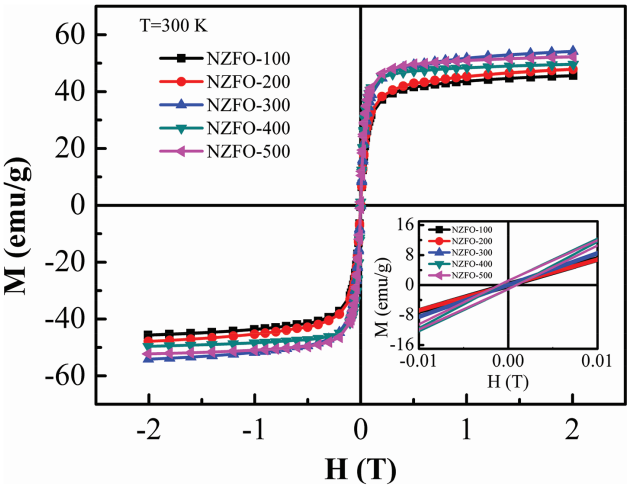

Figure 6: Room-temperature *M-H* loops for NZFO ferrites with different reactant concentrations. The inset shows the corresponding magnified view of the *M-H* curves at lower applied field.

where $\mu = M_s\pi D^3/6$ is the true magnetic moment of each particle, M_s is the saturation magnetization, k_B is the Boltzmann constant and T is the absolute temperature. The fit results of room-temperature *M-H* loops are displayed in Figure 7, and the values of M_s are listed in Table 1. It is observed that the measured values of M_s are considerably lower than that of the corresponding bulk material (86 emu/g) [23]. When the particle size decreases into nanometer-sized scale, surface area increases, which enhances the system energy and surface effect, making cation redistribution possible. Thus, the lower measured value of M_s is most likely attributed to cation redistribution. The value of M_s increases from 44.5 to 52.6 emu/g as the crystalline size increases from 17 to 22 nm. Such increases are usually explained as a decreasing proportion of the pinned surface magnetic moments in overall magnetization as the crystallites grow in size [24, 25]. Hollow NZFO-300 nanospheres, with a diameter of about 125 nm, possesses the highest M_s of 52.6 emu/g, and the results have a good agreement with that reported previously [13, 16, 26, 27]. The high M_s with hollow structure may be caused by the peculiar hollow structures and the distribution of metal ions on A and B sites of the spinel ferrite [16]. However, the M_s value is decreased when the crystalline size increases to 31 nm, which could be explained by the multidomain structure and the increase of the demagnetizing factor.

The magnetization curves of the NZFO nanoparticles prepared under different reactant concentrations at 10 K are shown in Figure 8. Below the blocking temperature, the thermal activation is no longer able to overcome the

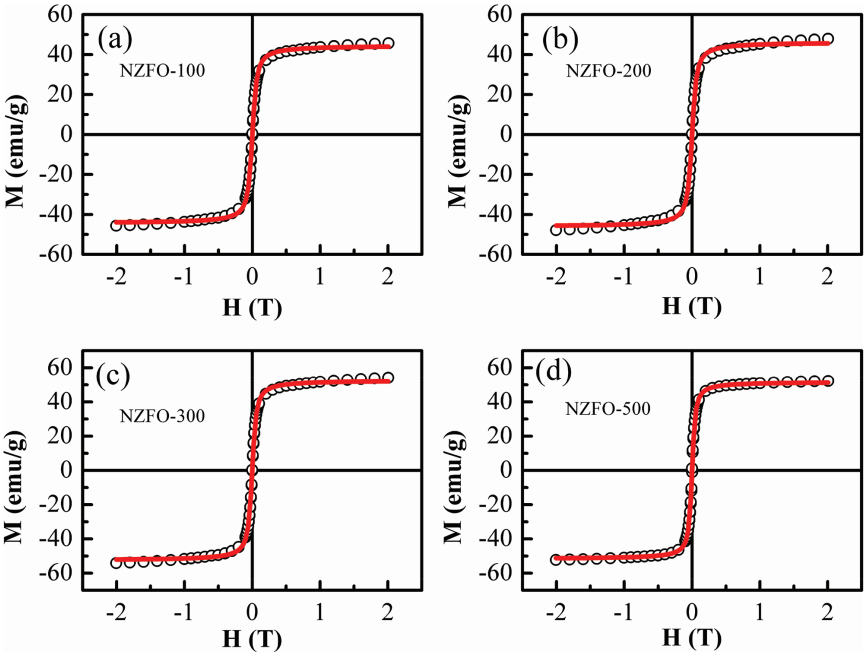

Figure 7: The nonlinear curve fit of Langevin function for the NZFO-100, NZFO-200 NZFO-300 and NZFO-500 samples.

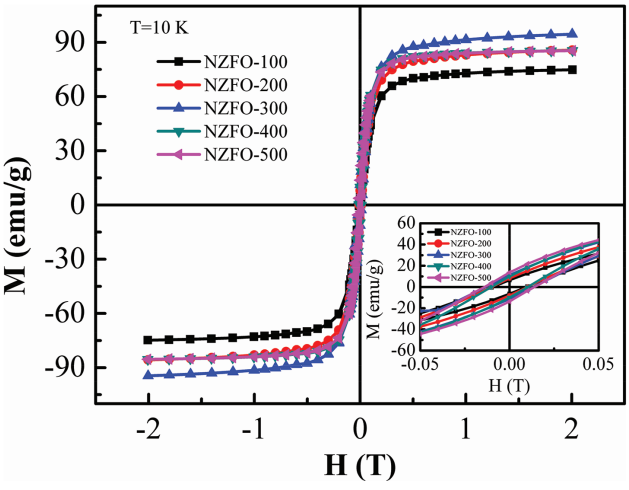

Figure 8: The *M-H* loops for NZFO ferrites at different reactant concentrations at 10 K. The inset shows the corresponding magnified view of the *M-H* curves at lower applied field.

magnetocrystalline anisotropy. Therefore, the NZFO nanoparticles show typical hysteresis behaviors, as shown in inset of Figure 8.

Conclusions

In summary, we have synthesized the monodisperse $Ni_{0.5}Zn_{0.5}Fe_2O_4$ nanospheres by one-step solvothermal method. The variation of crystallite size and nanospheres size can be adjusted by controlling reactant concentration. SEM and TEM characterizations confirm hollow structure of NZFO-300 nanospheres. Room-temperature superparamagnetic behaviors of synthesized samples are confirmed by magnetic measurement. The prepared hollow magnetite spheres exhibit high saturation magnetization of 52.6 emu/g at room temperature, which may be induced by the distribution of metal ions on A and B sites. Our study demonstrates the monodisperse $Ni_{0.5}Zn_{0.5}Fe_2O_4$ nanospheres may be potential candidates for application as biomedicine and magnetic fluid.

Funding: This work was financially supported by the Foundation of Educational Commission of Anhui Province (KJ2016B004), Anhui Provincial Natural Science Foundation (1508085ME100) and key technical project of Huaibei City (20140311).

References

[1] M.M. Rashad, D.A. Rayan, A.O. Turky, et al., J. Magn. Magn. Mater., 374 (2015) 359–366.
[2] S.D. Shenoy, P.A. Joy and M.R. Anantharaman, J. Magn. Magn. Mater., 269 (2004) 217–226.
[3] N. Ponpandian, A. Narayanasamy, C.N. Chinnasamy, et al., Appl. Phys. Lett., 86 (2005) 192510.
[4] M. Zhang, Q.C. Liu, Z.F. Zi, et al., Sci. China Tech. Sci., 56 (2012) 13–19.

[5] G.S. Shahane, A. Kumar, M. Arora, et al., J. Magn. Magn. Mater., 322 (2010) 1015–1019.
[6] C. Srinivas, B.V. Tirupanyam, A. Satish, et al., J. Magn. Magn. Mater., 382 (2015) 15–19.
[7] X. Li, Q. Li, Z. Xia, et al., J. Alloys Compd., 458 (2008) 558–563.
[8] S.A. Morrison, C.L. Cahill, E.E. Carpenter, et al., J. Appl. Phys., 95 (2004) 6392–6395.
[9] L.-Z. Li, L. Peng, X.-X. Zhong, et al., Ceram. Int., 42 (2016) 13238–13241.
[10] H.-W. Wang and S.-C. Kung, J. Magn. Magn. Mater., 270 (2004) 230–236.
[11] C.-R. Lin, I.H. Chen, C.-C. Wang, et al., Acta Mater, 59 (2011) 6710–6716.
[12] J. Gu, S. Li, M. Ju, et al., J. Cryst. Growth, 320 (2011) 46–51.
[13] W. Jiang, Z. Cao, R. Gu, et al., Smart Mater. Struct., 18 (2009) 125013.
[14] M. Zhang, X.-W. Gao, Z.F. Zi, et al., Electrochim. Acta, 147 (2014) 143–150.
[15] C. Venkataraju, G. Sathishkumar and K. Sivakumar, J. Magn. Magn. Mater., 322 (2010) 230–233.
[16] X. Lin, G. Ji, Y. Liu, et al., Cryst. Eng. Comm., 14 (2012) 8658.
[17] C. Vázquez-Vázquez, M.A. López-Quintela, M.C. Buján-Núñez, et al., J. Nanopart. Res., 13 (2010) 1663–1676.
[18] Y.F. Deng, Q.M. Zhang, S.D. Tang, et al., Chem. Commun., 47 (2011) 6828–6830.
[19] C. Caizer, Mater. Sci. Eng., B, 100 (2003) 63.
[20] A.S. Albuquerque, J.D. Ardisson, W.A.A. Macedo, et al., J. Appl. Phys., 87 (2000) 4352–4357.
[21] D.L. Leslie-Pelecky and R.D. Rieke, Chem. Mater., 8 (1996) 1770–1783.
[22] D.G. Chen, X.G. Tang, J.B. Wu, et al., J. Magn. Magn. Mater.323 (2011) 1717–1721.
[23] V. Sreeja, S. Vijayanand, S. Deka, et al., Hyperfine Interact, 183 (2008) 271–279.
[24] Q. Song and Z.J. Zhang, J. Am. Chem. Soc., 126 (2004) 6164–6168.
[25] S. Ayyappan, S. Mahadevan, P. Chandramohan, et al., J. Phys. Chem. C, 114 (2010) 6334–6341.
[26] F. Wang, J. Liu, J. Kong, et al., J. Mater. Chem., 21 (2011) 4314.
[27] A.G. Yan, X.H. Liu, R. Yi, et al., J. Phys. Chem. C, 112 (2008) 8558–8563.